THE JOURNAL OF PHYSICAL CHEMISTRY B

Article

pubs.acs.org/JPCB

Compression of High Grafting Density Opposing Polymer Brushes Using Molecular Dynamics Simulations in Explicit Solvent

Ian G. Elliott, Tonya L. Kuhl, and Roland Faller*

Department of Chemical Engineering & Materials Science, UC Davis, One Shields Avenue, Davis, California 95616, United States

ABSTRACT: Opposing polymer brush layers at high grafting density were examined under confinement and characterized with respect to structure and interaction forces using molecular dynamics simulations in an explicit solvent. The brush system underwent a static compression, where the system is simulated at several discrete separation distances. These simulations are all at the same solvent chemical potential as a non-interacting reference state to produce a realistic compression. Normal pressure−distance profiles were generated and compared to density profiles at each separation distance to determine structure−property relationships. Significant interpenetration of brush layers occurred at high compression, to the extent that each brush reached the opposing surface. Higher interpenetration corresponded to a sharp increase in the pressure−distance curve, suggesting a correlation between interpenetration and interaction forces. We find clear differences from literature values using implicit solvent techniques.

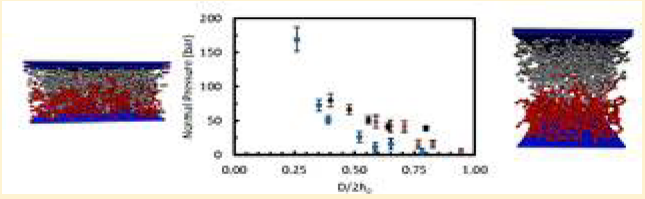

INTRODUCTION

A polymer brush consists of polymer chains end grafted to a surface. Crowding from the molecules at the surface leads to chain extension away from the surface, and numerous useful properties.[1,2] Polymer brushes can be used to modify surface properties and interactions to change the nature of the surface. Applications which take advantage of surface modification by polymer brushes include altering wetting properties,[3] biocompatiblizing surfaces or devices,[4] and reducing friction between surfaces.[5−8] The latter application is gaining increasing attention, as opposing polymer brushes have been shown to significantly lower friction, therefore acting as a viable lubricant for various applications.[9] The first step in taking advantage of the lubricating properties of polymer brushes is to thoroughly understand how the brushes interact when brought into confinement opposed to one another. Polymer brushes are typically characterized by either structure or interaction forces. Experimentally, this is achieved by neutron reflectivity to determine density profiles[10,11] and by the surface force apparatus to determine forces.[12−16] Also, atomic force microscopy can determine these forces.[17,18] In addition to experiments, there has been significant theoretical[19−21] and simulation[22−26] work on characterizing and predicting the structure and interactions of polymer brushes.

Molecular simulations have the advantage of obtaining high resolution structure and force information simultaneously. As all particle locations are always known, structure can be investigated at points of interest dictated by the force measurements. In this way, force data can be understood by linking it to structural features.

This paper details static compression of polymer brushes in an explicit solvent. Often simulations will investigate confined brushes without explicit solvent,[6,27−29] as this both simplifies and speeds up the simulations. Doing so, however, sacrifices detail about how the solvent responds in these circumstances. Some simulations[30−33] have included explicit solvent but upon compression maintained a constant total number density, not exactly reproducing conditions found in an experiment. Constant chemical potential simulations have been conducted using dissipative particle dynamics,[34−36] but again, these do not contain as much detail on the solvent as explicit solvent simulations. This work differs from previous studies in that it characterizes high grafting density opposing polymer brushes with explicit solvent, where the solvent density is determined on the basis of maintaining constant solvent chemical potential at all levels of compression.[37] The solvent chemical potential in all compressed cases is equal to that of a fully separated reference system, and thus, all compressed systems can be considered equilibrated with one another. This process approximates a compression in the grand canonical ensemble but is conducted by a series of NVT simulations.

SIMULATION DETAILS

All simulations were conducted with Gromacs 4.0.4.[38] The coarse-grained MARTINI[39] model (version 1.4) was used, which allows for much longer simulation times and larger systems. While originally developed for lipids, this model has been effectively used previously for polymer systems.[40−43] In this model, all particles are set to a mass of 72 g/mol and are assigned Lennard-Jones interactions which produce generically polar, nonpolar, or charged particles. For this study, all particles were polar. The polymer and solvent particles had equivalent interactions, and the surface was made of particles which, while

Received: November 30, 2012
Revised: March 18, 2013
Published: March 21, 2013

 © 2013 American Chemical Society dx.doi.org/10.1021/jp3118117 | J. Phys. Chem. B 2013, 117, 4134−4141

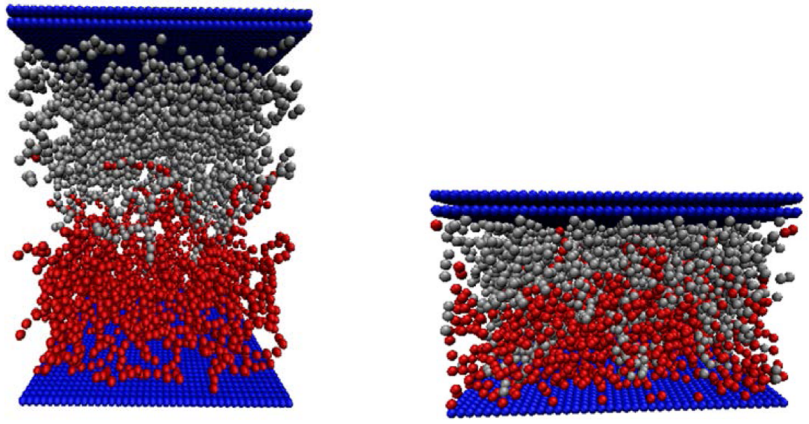

Figure 1. Images obtained with the VMD software[45] of the opposing polymer brush system at two levels of compression with separation distances of 15 nm (left) and 6.75 nm (right). Solvent molecules have been removed for clarity; the different brushes are shown in different color. This system has a grafting density of 0.347 chains/nm^2 with 40 monomer long chains.

still polar, had one-third the nonbonded interactions of the solvent and polymer.[42] The surface was composed of overlapping frozen particles spanning 12 nm by 12 nm in the x and y directions, which was the total area of the simulation box. It consisted of three surface layers to ensure there were no interactions through the z periodic boundary. To create a brush system, one end of each polymer was fixed 0.3 nm above either surface in a regular grafting pattern. All nonbonded interactions between frozen particles were omitted. Each simulation was initialized with a steepest descent energy minimization, followed by a brief simulation with a small time step of 0.001 ps. Simulations used for the production runs had a time step of 0.02 ps. Temperature was held constant at 350 K for all simulations using a Berendsen thermostat[44] with a correlation time of 1 ps. Previous work has shown that, at these temperatures, the polymer brushes are in a good solvent condition.[42] In simulations that were pressure coupled, a Berendsen barostat[44] was used with a correlation time of 2 ps. The neighbor list was updated every 10 steps and had a 1.4 nm cutoff length. The cutoff distance for Lennard-Jones interactions was 1.2 nm. Further details concerning this model can be found in refs 37 and 40.

The polymer brush systems studied consisted of 40 monomer long linear chains at grafting densities of 0.347 and 0.694 chains/nm^2, along with one longer chain system with 71 monomer chains at a grafting density of 0.347 chains/nm^2. Images of the short chain, low grafting density system at two different levels of compression are shown in Figure 1.

Single equilibrium brushes of both grafting densities with 40 monomer chains were thoroughly characterized previously using the same model,[42] so the focus here was on the effects of confinement. A measure of the degree to which the chains interact laterally is the overlap grafting density. Overlap grafting density can be represented by eq 1.

$$\sigma^* = \pi R_g{}^2 \Sigma \tag{1}$$

Σ is the grafting density in chains/area, and R_g is the radius of gyration calculated from a simulation of a single free polymer chain in solution. For $\sigma^* > 1$, the system is in the brush regime, where high lateral interaction will cause the chains to extend from the surface.[46] Grouping both chain length and grafting density into one term suggests that they have a similar impact. For example, if the values were selected to yield the same overlap grafting density, short chains at a high grafting density should have a similar structure as long chains at low grafting density. The effect of different systems with the same overlap grafting density was considered in this work. The system parameters are provided in Table 1. As shown in Table 1, two of the systems characterized had approximately the same overlap grafting density but arrived at that value by different chain lengths and grafting densities. These systems were used to determine if polymer brushes with the same overlap can be straightforwardly compared.

Table 1. Systems Examined in Terms of Grafting Density and Chain Length

system	grafting density Σ (chains/nm^2)	monomers per chain	overlap grafting density σ^*
A	0.347	40	6.97
B	0.694	40	13.93
C	0.347	71	13.79

To generate a reference system of unperturbed brushes, opposing brushes were set up for each overlap grafting density with a large enough separation distance such that the two brushes did not interact. The surfaces and brushes were initially placed in the center of the box so pressure coupling in the z direction could be applied without interference from fixed surface particles, as pressure coupling changes the box height. A simulation proceeded with the z pressure set to 1 bar for at least 100 ns. This was enough time for the z dimension of the box to stabilize, and the average box height after equilibration was used for further simulation with a fixed volume. An NVT simulation was conducted next for 2 μs, and data from the last 1.5 μs was used as the reference system. This process was conducted for each system A, B, and C.

All compressed systems were initially solvated to an arbitrary density and run for 2 μs. The chemical potential was calculated for each system to determine if more or less solvent particles were required to match the reference system's chemical potential. The details of this procedure have been thoroughly covered in a previous publication,[37] so they are only briefly summarized here. Essentially, chemical potential has two components: ideal and excess. The ideal component is based on the concentration of solvent particles. The excess chemical potential was determined using the test particle insertion

dx.doi.org/10.1021/jp3118117 | J. Phys. Chem. B 2013, 117, 4134−4141

method developed by Widom.[47] In this method, theoretical solvent particles are randomly added to the system and their interaction energy with all particles in the system is calculated. Enough insertions must occur in each frame of the trajectory such that the ensemble average is stable. The frequency of frames analyzed depends on the desired accuracy. For this work, the frequency ranged from 0.1 to 1 ns, with more frames required for highly compressed systems.

The values of solvent chemical potential obtained from the insertion calculations indicate if solvent particles need to be added or removed for the confined system to be in equilibrium with the reference system. After the initial simulation, the solvent density was adjusted accordingly, the simulation was run again, and the chemical potential was recalculated by the test particle insertion method. Once the difference between the solvent chemical potential of the reference system and the compressed system was close to zero, the system was considered in equilibrium with the other states and was analyzed for structural and force properties.

RESULTS

The first step in simulating a static compression was to determine the correct solvent density of each compressed system. Solvent chemical potential was extremely sensitive to solvent density, to the point where even minor changes in the number of solvent particles could strongly affect both the chemical potential and normal pressure. To illustrate this sensitivity, system A at a separation distance of 6.75 nm is used as an example. The system had roughly 4000 solvent particles and 4000 polymer beads at this separation. When at equilibrium with the reference system, the normal pressure was 73 bar and the solvent chemical potential was −0.02kT. Two systems at nearly the same density had also been set up. One had 23 solvent particles less than the correct system, and one had 27 particles more. These two systems deviated significantly in normal pressure from the 73 bar observed in the correct system. The system with 23 fewer solvent particles dropped to 38 bar and −0.09 kT, and the system with 27 more particles shot up to 118 bar and a chemical potential of 0.1 kT. So even an apparently small change of 20−30 particles has a significant impact in a system with 8000 particles to bring the system substantially out of equilibrium with the reference state, and completely change the pressure obtained. This makes sense, as 30/8000 particles multiplied with a modulus (inverse compressibility) of 1 GPa (see the compressibility discussion below) comes to 37.5 bar change, which is line with the observations. Clearly, the solvent density strongly affected the normal pressure, so the systems had to be set up with very little error in the chemical potential to get a meaningful value for pressure.

From these data points, an uncertainty in pressure for system A can be estimated on the basis of the uncertainty in the chemical potential calculation. Not all simulations of different separation distances had multiple runs, so the exact effect of adding or removing particles cannot be determined for each separation distance individually. However, for all systems where there is data for different solvent densities, a pressure change of 4−5 bar was associated with a 0.01 kT change in chemical potential. This was true for systems at both high and low confinement. A reasonable estimation for the error in pressure in system A can be made by using the average value of 4.65 bar change in normal pressure per 0.01 kT change in solvent chemical potential. It was decided therefore that the allowable error in chemical potential would be 0.02 kT and that all systems had also to be within 0.02 kT of the reference system's solvent chemical potential, yielding an error in pressure less than 10 bar. The only exception to this was the most compressed system (5 nm separation distance), as it finished within 0.03 kT of equilibrium, and at such a high level of compression was much more sensitive to density changes. For the higher density systems (B and C), the error was likewise determined but in all cases was in the range of 3−5 bar per 0.01 kT error in chemical potential.

Normal pressure versus distance profiles were created by calculating pressure profiles[48−50] at each separation distance to omit surface effects. An example of a normal pressure profile is shown in Figure 2. As can be seen, the pressure within the surface layers deviates dramatically from the average pressure in the rest of the system. To calculate the normal pressure for each system, the pressure profile was averaged between the surfaces, omitting any volume that the surface extended into. After averaging, the pressure of the reference system was subtracted from the normal pressure of all confined systems to yield pressure values relative to the non-interacting system.

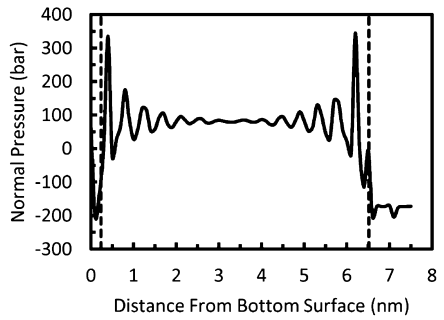

Figure 2. Normal pressure profile for system A with a surface separation of 6.75 nm. Dashed lines indicate where the surfaces extend in the system.

The average pressure itself for any given separation remained stable through the course of the simulation but as stated before has an error associated with how accurately the system was set up. Each pressure−distance profile has error bars for each of the data points based on the uncertainty in the chemical potential. Often, it is useful to plot data with distances relative to twice the uncompressed brush height, or where the opposing brushes should first start to interact. The uncompressed brush heights were calculated by eq 2[51,52] from a non-interacting system.

$$h_0 = \frac{8}{3}\langle z \rangle = \frac{8}{3}\frac{\int_0^\infty z\phi(z)\,\mathrm{d}z}{\int_0^\infty \phi(z)\,\mathrm{d}z} \tag{2}$$

In eq 2, ϕ is the polymer density profile and z is the distance from the bottom surface. The brush heights for systems A, B, and C were 9.60, 10.61, and 15.67 nm, respectively.

Figure 3 shows the normal pressure as a function of separation between the walls for the three systems. In addition, comparisons (both in linear and logarithmic scale) to simulations in implicit good solvent by Kreer et al. are shown.[23] The change of normal pressure with distance in our model is much less pronounced as in the case of implicit solvent. This is understandable when considering that the solvent modeled here is load bearing, whereas an implicit

dx.doi.org/10.1021/jp3118117 | J. Phys. Chem. B 2013, 117, 4134−4141

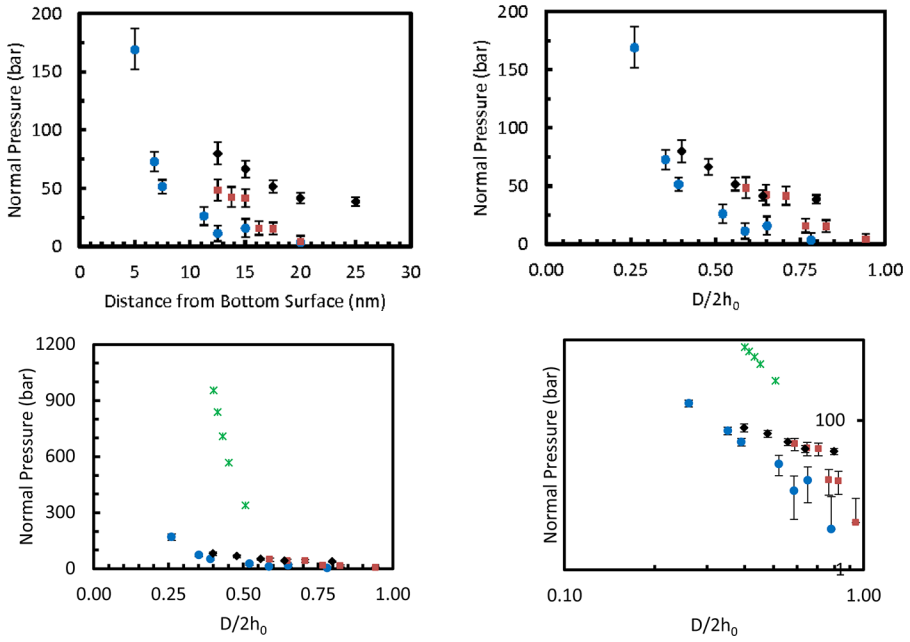

Figure 3. Normal pressure versus separation distance for each system under different levels of confinement. The plot on the left shows the pressure for each separation distance, while the right plot rescales the distance based on each system's uncompressed brush height. In the bottom figures, we compare our data (both linear and double logarithmic) with literature data from Kreer et al.[23] which was determined for 30 monomer chains at a grafting density (in our units) of 0.72 chains/nm^2 in an implicit good solvent. The uncompressed brush height was taken as 19.7σ (estimated from the density profile). The pressure scaling is based on the mapping that 800 bar corresponds to one dimensionless pressure unit (ε/σ^3 = 5 kJ/mol/(0.47 nm)^3), as these are the ε and σ values used in our simulations. Even if the y-axis was arbitrarily scaled, the increase of normal pressure with distance would be much steeper (see the logarithmic plot). Systems A, B, and C and literature data are represented by blue circles, red squares, black diamonds, and green stars, respectively.

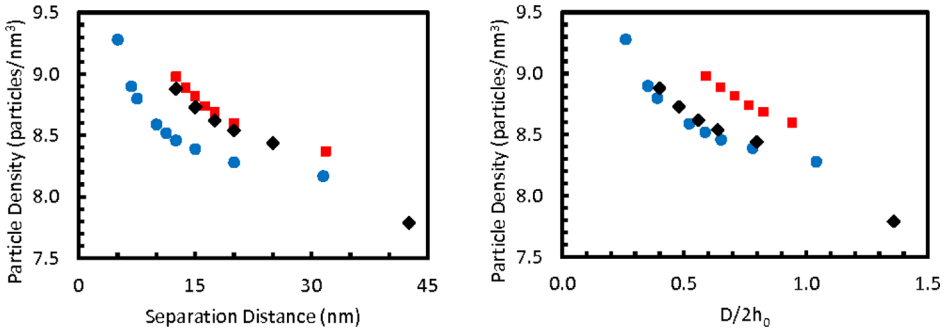

Figure 4. Total particle number density, including both polymer and solvent, for each separation distance (left) and rescaled relative to twice the brush heights (right) in equilibrium with the reference system. Error bars are smaller than the symbols. Systems A, B, and C are represented by blue circles, red squares, and black diamonds, respectively.

solvent is not. This means that a realistic solvent can already transmit forces at larger distances and therefore the increase is smoother. Additionally, the implicit solvent does not transmit attractive forces which are present in our model.

As much of the work associated with these simulations was setting up the systems at the correct density, it is informative to look at how the density changes with compression. All polymer beads and solvent particles were the same mass and size, so density is represented as a number density in particles/nm^3. The total particle density versus separation distance is shown in Figure 4. Clearly, the density increases throughout the compression. This suggests that using the constant density approximation is inadequate to realistically represent the physics of the compression.

One additional way this data can be examined is as what density the system adopts for a given pressure. Particle density versus normal pressure for all systems is shown in Figure 5.

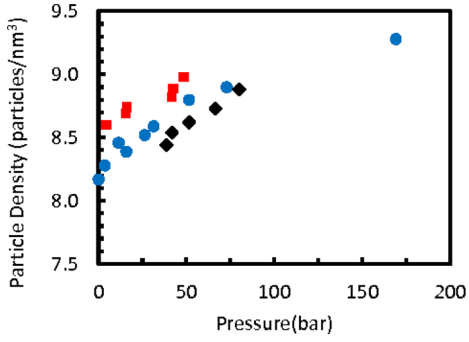

Figure 5. Total particle density versus normal pressure. Systems A, B, and C are represented by blue circles, red squares, and black diamonds, respectively.

dx.doi.org/10.1021/jp3118117 | J. Phys. Chem. B 2013, 117, 4134−4141

Density changes in response to pressure changes relate to the compressibility of the fluid. The isothermal compressibility is expressed in terms of density:

$$\kappa_T = \frac{1}{\rho}\left(\frac{\partial \rho}{\partial p}\right)_T \tag{3}$$

In eq 3, κ_T is the isothermal compressibility, ρ is the total density, and p is the normal pressure. Using the data from Figure 5 in eq 3, compressibility can be estimated. Using any of the three systems leads to a compressibility on the order of 10^{-4} bar^{-1}. When compared to available compressibility data, it is observed that this is about an order of magnitude higher than what is generally observed (order 10^{-5} bar^{-1}).[53,54] The increased compressibility is likely an artifact of the coarse-grained model, which does not exactly reproduce experimental conditions. This model leads to solvent layering at high compressions, which allows the system to be more highly compressed. Still, we are more realistic than calculating compressibility in a system without explicit solvent, as in that case the solvent is infinitely compressible and therefore only the polymer contributes. Additionally, in many solvent free models, attractive interactions are neglected.

Interesting features concerning the structure of the opposing brush systems can be elucidated by examining the brush density profiles. Figure 6 shows the density profile of a brush layer as it is compressed by the opposing brush.

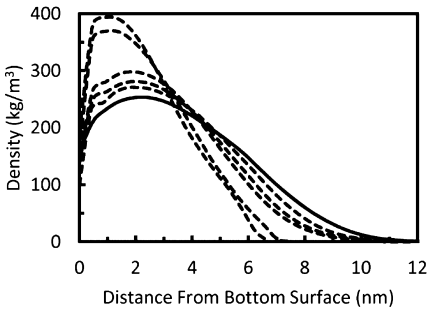

Figure 6. Density profile of a brush layer (system A) at different stages of compression. The solid line represents the equilibrium brush density profile for an uncompressed single brush from earlier studies.[42] All dashed lines are for the system as it compresses which correspond to surface separations of 6.75, 7.5, 11.25, 12.5, and 15 nm going from left to right.

The most noticeable change in structure from the uncompressed system is a shift from a long tail in the density profile to a profile which goes more sharply to zero when highly confined. The compression progression represented by density profiles is shown in Figure 7. Both the overall density and the density of each individual layer are shown.

One characteristic that can be monitored throughout the compression is the interpenetration of the brushes. Interpenetration is the degree to which each brush extends into the opposing brush, and can be quantified by examining the amount that each individual density profile overlaps with the other. There are several ways to define interpenetration, and one method is to calculate the fraction of a brush layer that is past the midplane of the system which is quantified in eq 4.[8,22,55]

$$I(D) = \frac{\int_{D/2}^{D} \phi(z)\, dz}{\int_{0}^{D} \phi(z)\, dz} \tag{4}$$

D is the separation between surfaces, ϕ is the volume fraction of polymer, and z is the distance from the bottom surface. Interpenetration data using eq 4 is shown in Figure 8.

Figure 8 quantitatively represents interpenetration as the fraction of polymer brush past the midplane. The interpenetration is insignificant at large separation distances, but under higher confinement, interpenetration increases substantially. In fact, interpenetration grows to the point where each brush extends completely through the opposing brush, as is seen in the density profiles in Figure 7. In the three most confined levels for system A, each brush passes all the way through the other brush and interacts with the opposing wall. The point at which each polymer layer extends to the other surface also corresponds to the level of confinement where substantial repulsive pressures are observed in Figure 3. Another way to describe the density profile at this point is that there is no longer a minimum in the overall density profile in the middle. Essentially, at this level of compression, the structure no longer is distinguishable as two separate brushes but more resembles one very high density brush confined between two surfaces.

Solvent density profiles can also be calculated to examine how the solvent behaves under confinement. Figure 9 shows the solvent densities for a low and highly compressed system.

For both levels of confinement, there is a significant peak in the solvent density profile near the surface. This indicates a polymer depletion layer, which persists even when the system is very highly compressed. At a high level of compression, the solvent starts to layer, which explains the higher compressibility obtained using this model.

An additional structural feature which can be examined is the chain end distribution. This distribution represents the behavior

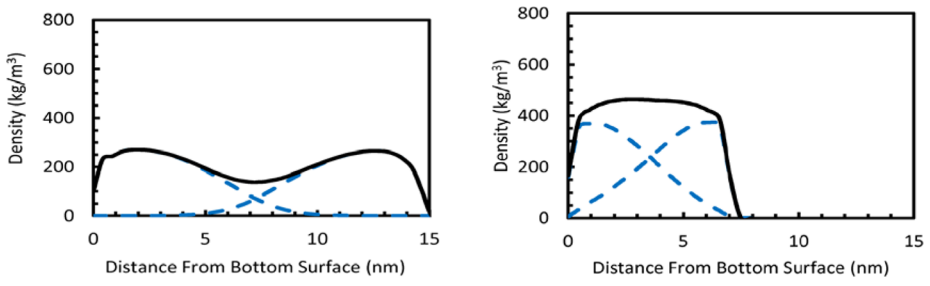

Figure 7. Density profiles for system A at two stages (15 and 7.5 nm separation distance) in the compression. The solid black line represents the total polymer density, while the dashed blue lines represent each individual brush layer.

dx.doi.org/10.1021/jp3118117 | J. Phys. Chem. B 2013, 117, 4134−4141

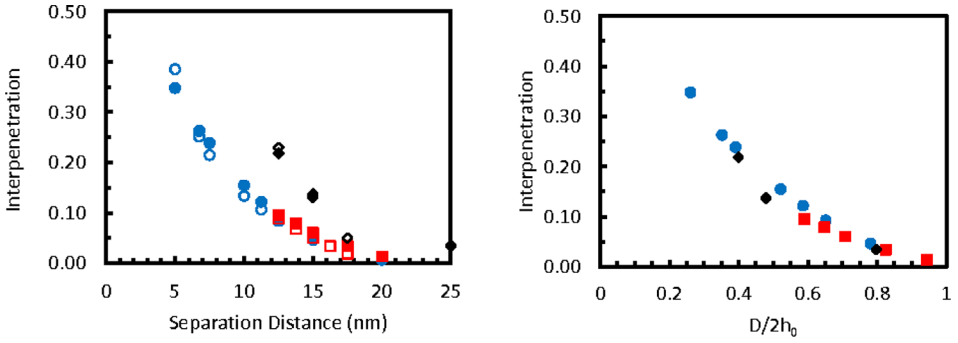

Figure 8. Interpenetration as defined by eq 4. Solid symbols represent interpenetration of the simulated systems, while open symbols show interpenetration as predicted by self-consistent field theory[55] for the same grafting density, chain length, and surface separation. Blue, red, and black represent systems A, B, and C, respectively. As only the dependence on surface separation was investigated here, the theoretical results were scaled by a common numerical prefactor for each system for comparison to the simulations.

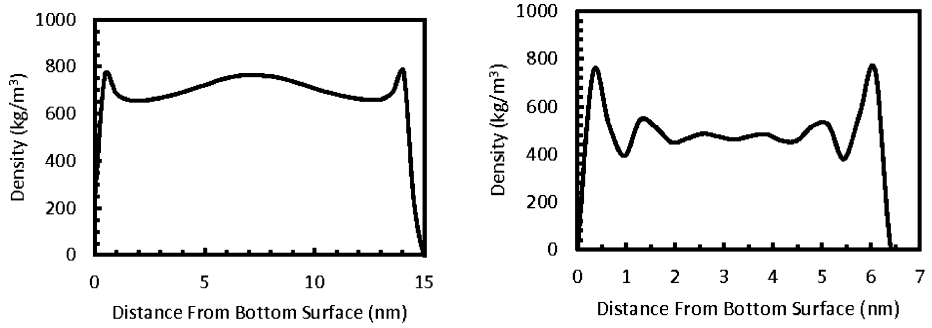

Figure 9. Solvent density profiles for 15 nm (left) and 6.75 nm (right) separation distances for system A.

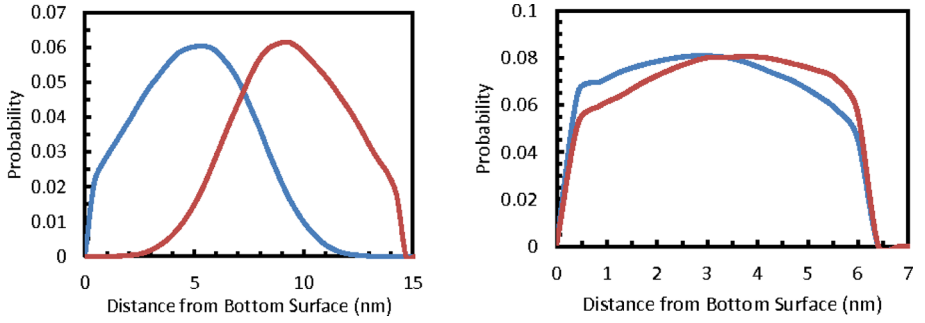

Figure 10. Chain end distributions for a low (left) and high (right) level of confinement for system A. Blue and red indicate the bottom and top brush chain ends, repectively. The chain end distribution was determined from the density profile of the last monomer of each chain, and normalized to a total probability of 1.

of the free end of each chain, illustrating if the chains have a tendency to collapse back into the brush or extend far away into the opposing layer. The distribution of each brush layer at both a high and a low level of confinement are shown in Figure 10.

From Figure 10, it can be seen that at lower levels of compression the chain end distributions have a definite peak; however, upon significant compression, the chain end distributions become much wider, indicating no significant preference throughout the brush.

CONCLUSIONS

Opposing polymer brushes were simulated and characterized under confinement at three different overlap grafting densities in the brush regime. A static compression was conducted where all separation distances examined are separate simulations. Using methods previously developed, a realistic confinement was achieved by requiring all simulations at different surface separations to be at the same solvent chemical potential. Both structure, in the form of density profiles, and the interactions between brush layers, represented by normal pressure, were examined for each separation distance. The total density of the system increased substantially with compression, indicating that a model allowing for changing density was indeed necessary. On the basis of the density change and measured pressures throughout the compression, this model overestimates the compressibility of the system compared to experimental data due to solvent layering in highly confined systems.

Comparing the change of normal pressure with distance to literature values, it is not as pronounced in this model as in the case of implicit solvent. This is understandable when considering that the solvent modeled here is load bearing, whereas an implicit solvent is not.

Interaction forces were calculated in the form of normal pressure versus distance plots. By comparing the normal

dx.doi.org/10.1021/jp3118117 | J. Phys. Chem. B 2013, 117, 4134−4141

pressure plot with the density profiles at each separation distance, structural explanations for observed trends in the normal pressure can be developed. The normal pressure experiences a large increase at the same time that interpenetration of the brush layers becomes more significant in the density profiles. When both brushes extend all the way through to the opposing surface, the normal pressure profile increases sharply. Being able to directly compare structure and forces simultaneously is a major benefit of simulations. While both of these characteristics can be measured experimentally, doing so in the same experiment would not be feasible. Interpenetration was calculated for each system to examine this observation further. It follows a monotonic increase with decreasing separation distance, and follows self-consistent field theory predictions qualitatively within a numerical constant.

The main effect of the compression on structure when compared to a single equilibrium brush is that the peak in the density profile becomes larger and the extended tail diminishes for each individual layer of the brush. Further, the chain end distributions have a single clear peak for each brush when interacting at larger separation distances, but this broadens under compression and is distributed across the entire box length. This indicates there is a mixture of chains that collapse back to the surfaces, extend through the opposing brush, and everything in between.

Future work will involve shearing the brushes at different separation distances to determine the lubrication properties of the brush, and how this changes with load. The systems are already set up at various separation distances at the correct solvent density, so the problem is greatly simplified.

AUTHOR INFORMATION

Notes

The authors declare no competing financial interest.

ACKNOWLEDGMENTS

We thank Torsten Kreer for interesting discussions and making his raw data available for comparison. This work was supported by the United States Department of Energy, Office of Basic Energy Science, under grant DE-FG02-06ER46340. I.G.E. additionally thanks the Graduate Assistance in Areas of National Need (GAANN) program of the U.S. Department of Education. Computer time at the National Energy Research Supercomputer Center, which is supported by the Office of Science of the U.S. Department of Energy under contract number DE-AC03-76SF00098, has been used for parts of the simulations.

REFERENCES

(1) Napper, D. H. *Polymeric Stabilization of Colloidal Dispersions*; Academic Press: London, 1983.

(2) Halperin, A.; Tirrell, M.; Lodge, T. *Tethered chains in polymer microstructures Macromolecules: Synthesis, Order and Advanced Properties*; Springer: Berlin/Heidelberg, 1992; Vol. *100*, p 31.

(3) Yokoyama, H.; Miyamae, T.; Han, S.; Ishizone, T.; Tanaka, K.; Takahara, A.; Torikai, N. Spontaneously Formed Hydrophilic Surfaces by Segregation of Block Copolymers with Water-Soluble Blocks. *Macromolecules* **2005**, *38*, 5180.

(4) Moro, T.; Takatori, Y.; Ishihara, K.; Konno, T.; Takigawa, Y.; Matsushita, T.; Chung, U.-i.; Nakamura, K.; Kawaguchi, H. Surface Grafting of Artificial Joints with a Biocompatible Polymer for Preventing Periprosthetic Osteolysis. *Nat. Mater.* **2004**, *3*, 829.

(5) Klein, J.; Kumacheva, E.; Perahia, D.; Mahalu, D.; Warburg, S. Interfacial Sliding of Polymer-Bearing Surfaces. *Faraday Discuss.* **1994**, *98*, 173.

(6) Grest, G. S. Interfacial Sliding of Polymer Brushes: A Molecular Dynamics Simulation. *Phys. Rev. Lett.* **1996**, *76*, 4979.

(7) Pelletier, E.; Belder, G.; Hadziioannou, G.; Subbotin, A. *Nanorheology of Adsorbed Diblock Copolymer Layers; HAL - CCSD*, 1997.

(8) Grest, G. Normal and Shear Forces between Polymer Brushes. *Adv. Polym. Sci.* **1999**, *138*, 149.

(9) Klein, J.; Kumacheva, E.; Mahalu, D.; Perahia, D.; Fetters, L. J. Reduction of Frictional Forces between Solid Surfaces Bearing Polymer Brushes. *Nature* **1994**, *370*, 634.

(10) Hamilton, W. A.; Smith, G. S.; Alcantar, N. A.; Majewski, J.; Toomey, R. G.; Kuhl, T. L. Determining the Density Profile of Confined Polymer Brushes with Neutron Reflectivity. *J. Polym. Sci., Part B: Polym. Phys.* **2004**, *42*, 3290.

(11) Ell, J. R.; Mulder, D. E.; Faller, R.; Patten, T. E.; Kuhl, T. L. Structural Determination of High Density, ATRP Grown Polystyrene Brushes by Neutron Reflectivity. *Macromolecules* **2009**, *42*, 9523.

(12) Klein, J.; Kamiyama, Y.; Yoshizawa, H.; Israelachvili, J. N.; Fredrickson, G. H.; Pincus, P.; Fetters, L. J. Lubrication Forces between Surfaces Bearing Polymer Brushes. *Macromolecules* **1993**, *26*, 5552.

(13) Watanabe, H.; Tirrell, M. Measurement of Forces in Symmetric and Asymmetric Interactions between Diblock Copolymer Layers Adsorbed on Mica. *Macromolecules* **1993**, *26*, 6455.

(14) Tian, P.; Uhrig, D.; Mays, J. W.; Watanabe, H.; Kilbey, S. M. Role of Branching on the Structure of Polymer Brushes Formed from Comb Copolymers. *Macromolecules* **2005**, *38*, 2524.

(15) Schorr, P. A.; Kwan, T. C. B.; Kilbey, S. M.; Shaqfeh, E. S. G.; Tirrell, M. Shear Forces between Tethered Polymer Chains as a Function of Compression, Sliding Velocity, and Solvent Quality. *Macromolecules* **2002**, *36*, 389.

(16) Liao, W.-P.; Kuhl, T. L. Steric Forces of Tethered Polymer Chains as a Function of Grafting Density: Studies with a Single Diblock Molecular Weight. *Macromolecules* **2012**, *45*, 5766.

(17) Pasche, S.; Textor, M.; Meagher, L.; Spencer, N. D.; Griesser, H. J. Relationship between Interfacial Forces Measured by Colloid-Probe Atomic Force Microscopy and Protein Resistance of Poly(ethylene glycol)-Grafted Poly(l-lysine) Adlayers on Niobia Surfaces. *Langmuir* **2005**, *21*, 6508.

(18) Sui, X.; Zapotoczny, S.; Benetti, E. M.; Schon, P.; Vancso, G. J. Characterization and Molecular Engineering of Surface-Grafted Polymer Brushes across the Length Scales by Atomic Force Microscopy. *J. Mater. Chem.* **2010**, *20*, 4981.

(19) Alexander, S. Adsorption of Chain Molecules with a Polar Head: a Scaling Description. *J. Phys.* **1977**, *38*, 983.

(20) de Gennes, P. G. Conformations of Polymers Attached to an Interface. *Macromolecules* **1980**, *13*, 1069.

(21) Milner, S. T.; Witten, T. A.; Cates, M. E. Theory of the Grafted Polymer Brush. *Macromolecules* **1988**, *21*, 2610.

(22) Murat, M.; Grest, G. S. Interaction between Grafted Polymeric Brushes: a Molecular-Dynamics Study. *Phys. Rev. Lett.* **1989**, *63*, 1074.

(23) Kreer, T.; Müser, M. H.; Binder, K.; Klein, J. Frictional Drag Mechanisms between Polymer-Bearing Surfaces. *Langmuir* **2001**, *17*, 7804.

(24) Dimitrov, D. I.; Milchev, A.; Binder, K. Polymer Brushes in Solvents of Variable Quality: Molecular Dynamics Simulations Using Explicit Solvent. *J. Chem. Phys.* **2007**, *127*, 084905.

(25) Pastorino, C.; Binder, K.; Müller, M. Coarse-Grained Description of a Brush−Melt Interface in Equilibrium and under Flow. *Macromolecules* **2008**, *42*, 401.

(26) Träskelin, P. T.; Kuhl, T. L.; Faller, R. Molecular Dynamics Simulations of Polystyrene Brushes in Dry Conditions and in Toluene Solution. *Phys. Chem. Chem. Phys.* **2009**, *11*, 11324.

(27) Chakrabarti, A.; Nelson, P.; Toral, R. Interpenetrations in Polymer Brushes. *J. Chem. Phys.* **1994**, *100*, 748.

(28) Neelov, I. M.; Binder, K. Brownian Dynamics Simulation of Grafted Polymer Brushes. *Macromol. Theory Simul.* **1995**, *4*, 119.
(29) Neelov, I. M.; Borisov, O. V.; Binder, K. Shear Deformation of Two Interpenetrating Polymer Brushes: Stochastic Dynamics Simulation. *J. Chem. Phys.* **1998**, *108*, 6973.
(30) Grest, G. S. Computer Simulations of Shear and Friction between Polymer Brushes. *Curr. Opin. Colloid Interface Sci.* **1997**, *2*, 271.
(31) Grest, G. S. In *Dynamics in Small Confined Systems III*; Drake, J. M., Klafter, J., Kopelman, R., Eds.; Materials Research Society: Pittsburgh, PA, 1997; Vol. *464*, p 71.
(32) Galuschko, A.; Spirin, L.; Kreer, T.; Johner, A.; Pastorino, C.; Wittmer, J.; Baschnagel, J. Frictional Forces between Strongly Compressed, Nonentangled Polymer Brushes: Molecular Dynamics Simulations and Scaling Theory. *Langmuir* **2010**, *26*, 6418.
(33) Spirin, L.; Galuschko, A.; Kreer, T.; Johner, A.; Baschnagel, J.; Binder, K. Polymer-Brush Lubrication in the Limit of Strong Compression. *Eur. Phys. J. E: Soft Matter Biol. Phys.* **2010**, *33*, 307.
(34) Goujon, F.; Malfreyt, P.; Tildesley, D. J. Dissipative Particle Dynamics Simulations in the Grand Canonical Ensemble: Applications to Polymer Brushes. *ChemPhysChem* **2004**, *5*, 457.
(35) Goujon, F.; Malfreyt, P.; Tildesley, D. J. Mesoscopic Simulation of Entangled Polymer Brushes under Shear: Compression and Rheological Properties. *Macromolecules* **2009**, *42*, 4310.
(36) Goujon, F.; Malfreyt, P.; Tildesley, D. J. Interactions between Polymer Brushes and a Polymer Solution: Mesoscale Modelling of the Structural and Frictional Properties. *Soft Matter* **2010**, *6*, 3472.
(37) Elliott, I. G.; Kuhl, T. L.; Faller, R. A Molecular Dynamics Technique to Extract Forces in Soft Matter Systems under Compression with Constant Solvent Chemical Potential. *J. Chem. Theory Comput.* **2012**, *8*, 1072.
(38) Hess, B.; Kutzner, C.; van der Spoel, D.; Lindahl, E. GROMACS 4: Algorithms for Highly Efficient, Load-Balanced, and Scalable Molecular Simulation. *J. Chem. Theory Comput.* **2008**, *4*, 435.
(39) Marrink, S. J.; de Vries, A. H.; Mark, A. E. Coarse Grained Model for Semiquantitative Lipid Simulations. *J. Phys. Chem. B* **2004**, *108*, 750.
(40) Hatakeyama, M.; Faller, R. Coarse-Grained Simulations of ABA Amphiphilic Triblock Copolymer Solutions in Thin Films. *Phys. Chem. Chem. Phys.* **2007**, *9*, 4662.
(41) Elliott, I. G.; Mulder, D. E.; Traskelin, P. T.; Ell, J. R.; Patten, T. E.; Kuhl, T. L.; Faller, R. Confined Polymer Systems: Synergies between Simulations and Neutron Scattering Experiments. *Soft Matter* **2009**, *5*, 4612.
(42) Elliott, I. G.; Kuhl, T. L.; Faller, R. Molecular Simulation Study of the Structure of High Density Polymer Brushes in Good Solvent. *Macromolecules* **2010**, *43*, 9131.
(43) Rossi, G.; Elliott, I. G.; Ala-Nissila, T.; Faller, R. Molecular Dynamics Study of a MARTINI Coarse-Grained Polystyrene Brush in Good Solvent: Structure and Dynamics. *Macromolecules* **2011**, *45*, 563.
(44) Berendsen, H. J. C.; Postma, J. P. M.; Gunsteren, W. F. v.; DiNola, A.; Haak, J. R. Molecular Dynamics with Coupling to an External Bath. *J. Chem. Phys.* **1984**, *81*, 3684.
(45) Humphrey, W.; Dalke, A.; Schulten, K. VMD: Visual Molecular Dynamics. *J. Mol. Graphics* **1996**, *14*, 33.
(46) Milner, S. T. Polymer Brushes. *Science* **1991**, *251*, 905.
(47) Widom, B. Some Topics in the Theory of Fluids. *J. Chem. Phys.* **1963**, *39*, 2808.
(48) Lindahl, E.; Edholm, O. Spatial and Energetic-Entropic Decomposition of Surface Tension in Lipid Bilayers from Molecular Dynamics Simulations. *J. Chem. Phys.* **2000**, *113*, 3882.
(49) Ollila, S.; Hyvönen, M. T.; Vattulainen, I. Polyunsaturation in Lipid Membranes: Dynamic Properties and Lateral Pressure Profiles. *J. Phys. Chem. B* **2007**, *111*, 3139.
(50) Ollila, O. H. S.; Risselada, H. J.; Louhivuori, M.; Lindahl, E.; Vattulainen, I.; Marrink, S. J. 3D Pressure Field in Lipid Membranes and Membrane-Protein Complexes. *Phys. Rev. Lett.* **2009**, *102*, 078101.
(51) Kreer, T.; Metzger, S.; Muller, M.; Binder, K.; Baschnagel, J. Static Properties of End-Tethered Polymers in Good Solution: A Comparison between Different Models. *J. Chem. Phys.* **2004**, *120*, 4012.
(52) Dimitrov, D. I.; Milchev, A.; Binder, K. Polymer Brushes in Cylindrical Pores: Simulation versus Scaling Theory. *J. Chem. Phys.* **2006**, *125*, 034905.
(53) Boyer, R. F.; Miller, R. L. Correlation of Liquid-State Compressibility and Bulk Modulus with Cross-Sectional Area per Polymer Chain. *Macromolecules* **1984**, *17*, 365.
(54) Kushare, S. K.; Terdale, S. S.; Dagade, D. H.; Patil, K. J. Compressibility and Volumetric Studies of Polyethylene-Glycols in Aqueous, Methanolic, and Benzene Solutions at T=298.15 K. *J. Chem. Thermodyn.* **2007**, *39*, 1125.
(55) Whitmore, M. D.; Baranowski, R. End-Anchored Polymers: Compression by Different Mechanisms and Interpenetration of Apposing Layers. *Macromol. Theory Simul.* **2005**, *14*, 75.